





## Article

# BaTiO<sub>3</sub> Functional Perovskite as Photocathode in Microbial Fuel Cells for Energy Production and Wastewater Treatment

Noureddine Touach<sup>1,\*</sup>, Abdellah Benzaouak<sup>1,\*</sup> , Jamil Toyir<sup>2</sup> , Youssra El Hamdouni<sup>1</sup>, Mohammed El Mahi<sup>1</sup>, El Mostapha Lotfi<sup>1</sup>, Najoua Labjar<sup>1</sup> , Mohamed Kacimi<sup>3</sup> and Leonarda Francesca Liotta<sup>4,\*</sup> 

- <sup>1</sup> Laboratory of Spectroscopy, Molecular Modelling, Materials, Nanomaterials, Water and Environment, Environmental Materials Team, ENSAM, Mohammed V University in Rabat, Avenue des Forces Armées Royales, Rabat B.P. 6207, Morocco
- <sup>2</sup> Laboratoire des Procédés, Matériaux et Environnement (LPME), Faculté Polydisciplinaire (FP-Taza), Faculté des Sciences Et Techniques de Fès (FST-Fès), Université Sidi Mohammed Ben Abdellah, Taza B.P. 1223, Morocco
- <sup>3</sup> Laboratory of Physical Chemistry of Materials, Catalysis and Environment, Department of Chemistry, Faculty of Sciences, Mohammed V University in Rabat, Rabat B.P. 1014, Morocco
- <sup>4</sup> Istituto per lo Studio dei Materiali Nanostrutturati (ISMN)-CNR, via Ugo La Malfa, 153, 90146 Palermo, Italy
- \* Correspondence: nour-eddine.touach@ensam.um5.ac.ma (N.T.); abdellah.benzaouak@ensam.um5.ac.ma (A.B.); leonardafrancesca.liotta@cnr.it (L.F.L.)

**Abstract:** Microbial fuel cells (MFCs) provide new opportunities for the sustainable production of energy, converting organic matter into electricity through microorganisms. Moreover, MFCs play an important role in remediation of environmental pollutants from wastewater with power generation. This work focuses on the evaluation of ferroelectric perovskite materials as a new class of non-precious photocatalysts for MFC cathode construction. Nanoparticles of BaTiO<sub>3</sub> (BT) were prepared and tested in a microbial fuel cell (MFC) as photocathode catalytic components. The catalyst phases were synthesized, identified and characterized by XRD, SEM, UV–Vis absorption spectroscopy, P-E hysteresis and dielectric measurements. The maximum absorption of BT nanoparticles was recorded at 285 nm and the energy gap (E<sub>g</sub>) was estimated to be 3.77 eV. Photocatalytic performance of cathodes coated with BaTiO<sub>3</sub> was measured in a dark environment and then in the presence of a UV–visible (UV–Vis) light source, using a mixture of dairy industry and domestic wastewater as a feedstock for the MFCs. The performance of the BT cathodic component is strongly dependent on the presence of UV–Vis irradiation. The BT-based cathode functioning under UV–visible light improves the maximum power densities and the open circuit voltage (OCV) of the MFC system. The values increased from 64 mW m<sup>-2</sup> to 498 mW m<sup>-2</sup> and from 280 mV to 387 mV, respectively, showing that the presence of light effectively improved the photocatalytic activity of this ceramic. Furthermore, the MFCs operating under optimal conditions were able to reduce the chemical oxygen demand load in wastewater by 90% (initial COD = 2500 mg L<sup>-1</sup>).

**Keywords:** microbial fuel cell; wastewater treatment; BaTiO<sub>3</sub>; photocathode; perovskite; chemical oxygen demand



**Citation:** Touach, N.; Benzaouak, A.; Toyir, J.; El Hamdouni, Y.; El Mahi, M.; Lotfi, E.M.; Labjar, N.; Kacimi, M.; Liotta, L.F. BaTiO<sub>3</sub> Functional Perovskite as Photocathode in Microbial Fuel Cells for Energy Production and Wastewater Treatment. *Molecules* **2023**, *28*, 1894. <https://doi.org/10.3390/molecules28041894>

Academic Editors: Lin Huang and Yinghuai Zhu

Received: 18 January 2023

Revised: 12 February 2023

Accepted: 13 February 2023

Published: 16 February 2023



**Copyright:** © 2023 by the authors. Licensee MDPI, Basel, Switzerland. This article is an open access article distributed under the terms and conditions of the Creative Commons Attribution (CC BY) license (<https://creativecommons.org/licenses/by/4.0/>).

## 1. Introduction

Sustainable development is crucial for addressing environmental and societal challenges such as climate change, population growth, and resource reduction. Nowadays, it is more necessary than ever to adopt highly efficient methods that take into account economic, social and environmental aspects, such as reducing emissions from fossil energy, promoting renewable energy and protecting biodiversity. In the current conjuncture of climate change and water crises, the development of technologies for the conversion of renewable energies, particularly the chemical energy of effluents into bioelectricity [1–3], has become, more than ever, a necessity. In this context, the microbial fuel cell technology appears as a promising

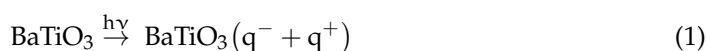
solution, capable of wastewater treatment and generating bioelectricity through the actions of microorganisms [4,5]. The large-scale implementation of this technology is directly related to the economic cost and efficiency of all the components of this system, in particular the cathode [6–8]. The design of an efficient air cathode for oxygen reduction (ORR) in microbial fuel cells (MFCs) is a crucial step in the building process of this technology [5,9]. The most active systems are mainly based on noble metals, in particular Pt, Rh and Pd. However, they are more and more expensive and difficult to access in the market, which can be a significant disadvantage when MFC devices come to be commercialized [10,11]. Thus, recently, the development is focused on the implementation of catalysts, based on non-precious metals, that are active, stable and less expensive [12]. However, despite this considerable progress, the activity and sustainability of tested catalysts for ORR are still insufficient.

Important electrode reactions including oxygen reduction reaction (ORR) and oxygen evolution reaction (OER) play a key role in driving the operating processes of air cathode biofuel cells. Inorganic perovskite oxides have been reported as effective systems for both ORR and OER [13,14]. Interestingly, oxygen-deficient perovskite catalysts such as  $\text{BaTiO}_{2.76}$  exhibit high catalytic activity simultaneously for the ORR and the OER. In these processes, surface and bulk oxygen diffusion through the solid is an important issue which can be improved using defective structure perovskites. These materials are well known to possess remarkable electronic and magnetic properties, in addition the presence of oxygen vacancies allowing high mobility of oxygen ions through the lattice [15,16].

Besides their ability to ensure an excellent mobility of oxygen ions, suitably prepared nanostructured perovskites can perform well as catalysts for ORR with low energy for oxygen activation and high electron transfer kinetics, resulting in a good electrocatalytic activity [17]. Recently, the potential of some ferroelectric perovskite electrodes has been investigated through electrocatalytic and photoelectrocatalytic tests carried out in single-chamber MFCs. Such perovskites were able to enhance the performance of MFCs and the energy recovery. It was reported that  $\text{LiNbO}_3$  cathodes exhibited a maximum power of  $131 \text{ mW m}^{-3}$  under irradiation and a maximum chemical oxygen demand (COD) removal of 84% [9]. In another study,  $\text{LiTaO}_3$ , a ferroelectric material, has shown good performances as a photocathode with a maximum generated power of  $55 \text{ mW m}^{-3}$  and a COD removal power of 66% [18]. The electrocatalytic performance of ceramic materials, such as  $(\text{Li}_{0.95}\text{Cu}_{0.15})\text{Ta}_{0.76}\text{Nb}_{0.19}\text{O}_3$  and  $\text{Li}_{0.95}\text{Ta}_{0.76}\text{Nb}_{0.19}\text{Mg}_{0.15}\text{O}_3$ , has also been investigated when used as photocathodes for MFCs. They can generate maximum powers of  $19.77 \text{ mW m}^{-3}$  ( $25.13 \text{ mW m}^{-2}$ ) and  $228 \text{ mW m}^{-2}$ , respectively [19–21] and percentages of 93% and 95.70% in terms of COD removal, thus showing good potential as photocathodes in MFC devices.

Among other ferroelectric perovskites, it is worth mentioning  $\text{BaTiO}_3$ , a functional ceramic, recognized for its ferroelectric properties resulting from distorted unit cells and the displacement of the positive and negative charge barycenter of the crystal [22]. Recently,  $\text{BaTiO}_3$  as a catalyst has attracted much attention, particularly for the reduction of  $\text{CO}_2$  to methanol [23], partial oxidation of methane [24], ammonia synthesis and toluene decomposition [25,26].  $\text{BaTiO}_3$  has also been widely studied in photocatalysis thanks to its internal electric field generated by permanent polarization [27,28] that enhances the separation of photo-induced charge carriers [29,30]. This material has been tested in several photocatalytic reactions, especially the degradation of organic dyes under white visible light [31–34]. According to the literature, the following reactions are the key steps of photo-induced reactions catalyzed by  $\text{BaTiO}_3$  [30,35]:

The absorption of photons by barium ( $h\nu \geq E_{\text{bg}} = 3.23 \text{ eV}$ ), Equation (1):



The negative charges ( $q^-$ ) can be rapidly trapped by molecular oxygen on the surface to form superoxide radical ( $O_2^{\bullet-}$ ), as shown in chemical Equation (2):



This radical could be combined with  $H^+$  coming from PEM to form  $H_2O_2$  Equation (3):



On these bases,  $BaTiO_3$  (BT) appears a very suitable material for electrocatalytic and photocatalytic applications. In the present study, we investigate, for the first time, the catalytic performance of  $BaTiO_3$  as a cathode for MFC devices, both in the presence and absence of UV-Vis light irradiation. The photocatalytic activity of this ferroelectric material, in terms of energy performance and wastewater purification, was studied in a single-chamber MFC fed with dairy industry and domestic wastewater.

## 2. Results and Discussion

### 2.1. Characterization of $BaTiO_3$ Structure and Morphology

The X-ray diffraction (XRD) technique was used to verify the purity of the synthesized phase and determine the crystalline structure of the  $BaTiO_3$  material. The diffraction pattern is shown in Figure 1. All the peaks are in good agreement with the reference, tetragonal perovskite structure with  $P4mm$  space group 3 (JCPDS No. 76-0744). Tetragonality can be confirmed by the peaks at specific angles, such as  $22.3^\circ$ ,  $31.6^\circ$ ,  $38.9^\circ$ ,  $45.3^\circ$ ,  $50.9^\circ$ ,  $54.1^\circ$ ,  $56.2^\circ$ ,  $65.9^\circ$  and  $70.3^\circ$   $2\theta$ . Such peaks were attributed to the (100), (101), (111), (200), (201), (211), (202), (212), (310) and (113) crystal planes, respectively. These observations are consistent with previous studies [30,36].

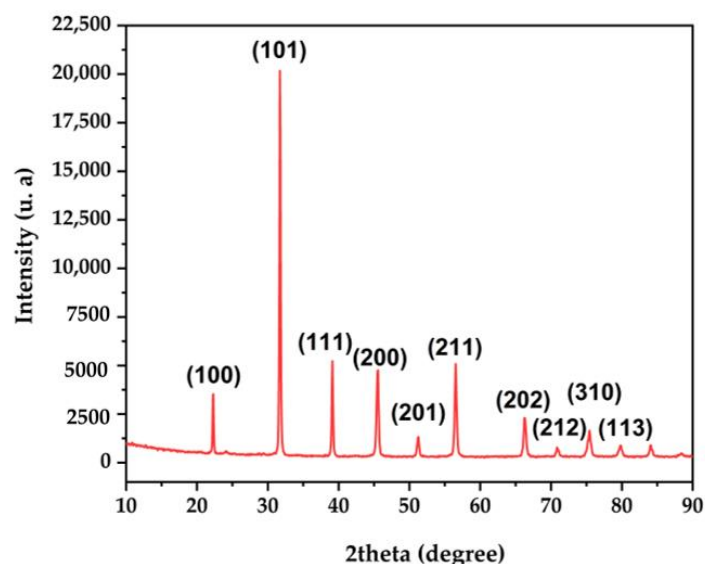


**Figure 1.** X-ray diffraction pattern of  $BaTiO_3$  powder.

Scanning electron microscopy (SEM) analyses were performed for detailed insights into the morphology of the prepared  $BaTiO_3$  sample. Figure 2a,b illustrates SEM images of the BT powder. As results from this microstructure analysis, the particles having nanometric sizes between 40 and 200 nm exhibited the crystalline shape of tetragonal parallelepipeds in agreement with XRD results. Furthermore, the elemental mapping SEM of Ba, Ti and O in Figure 2c–e indicates the homogeneous dispersion of these elements. The energy dispersive spectroscopy (EDS) results are illustrated in Figure 2b. From this analysis, the chemical composition of the prepared sample was revealed with high accuracy. The ratio between

the atomic percentages of Ba (18.5%), Ti (16.4%) and O (65.1%) is equal to 1.12:1:3.5, which is near the stoichiometric ratio of BaTiO<sub>3</sub>.

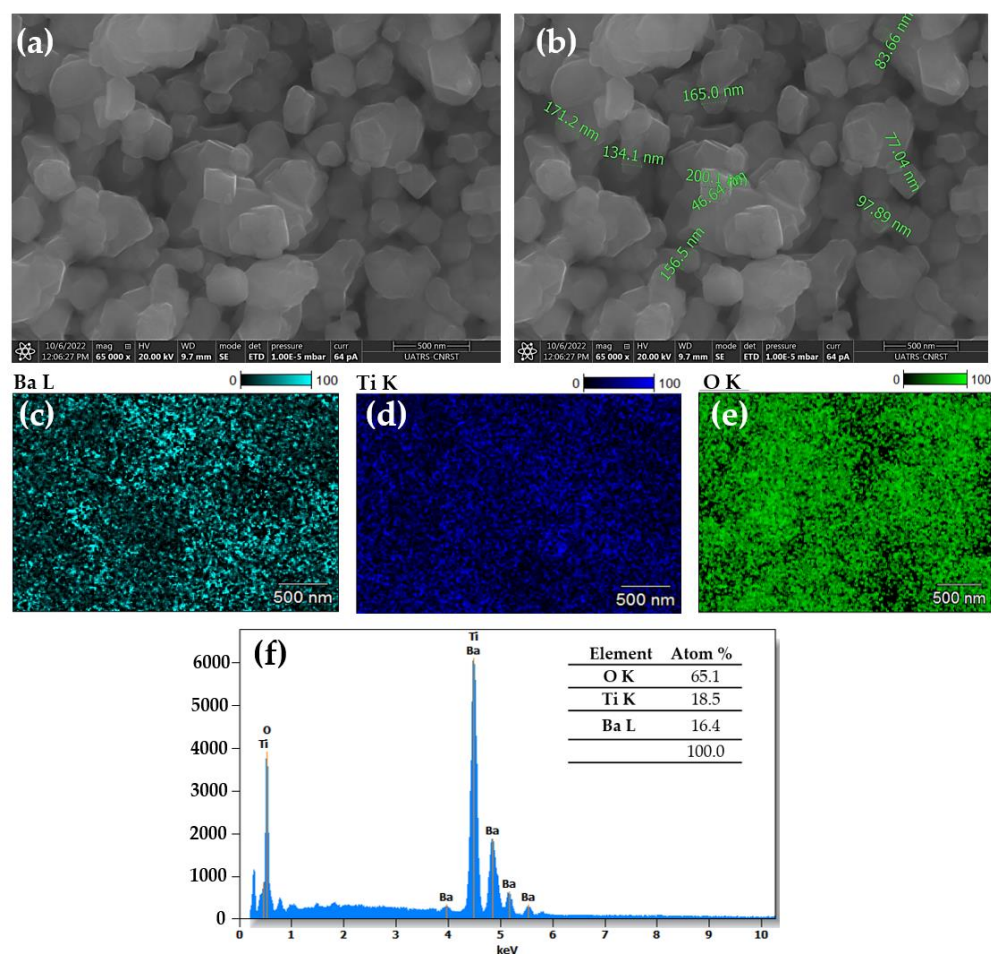


**Figure 2.** SEM images of BaTiO<sub>3</sub> powder (a,b), elemental mappings (c–e), EDS spectrum (f).

It is worth noting that BaTiO<sub>3</sub>, when is subjected to high temperatures or strong electric fields, can undergo distortion of the crystalline structure, changing its electrical and electronic properties. This distortion can lead to a change in polarization, which is related to the appearance of free electrical charges on the surface of the ceramic. This polarization change is responsible for the ferroelectricity of BaTiO<sub>3</sub> that is one of the most important properties of the material, particularly in catalysis [37].

The structural distortion of BaTiO<sub>3</sub> can also cause a change in the electronic energy bands, which can affect the electronic transport properties of the material. It might lead to an increase in the density of electronic states on the surface of the ceramic, improving the electrical conductivity.

In this regard, dielectric measurements for the prepared material (BT) were performed. The P-E hysteresis loop and dielectric response of the BT ceramic are plotted in Figure 3. As can be seen in Figure 3a, the material presents a typical P-E hysteresis loop at room temperature, with a remanent polarization value (Pr) of approximately 1.807  $\mu\text{C cm}^{-2}$ . It has been pointed out that the loop area of the material is relatively large, which confirms the relatively high dielectric constant. In addition, the dielectric response of the BT is also an important property, as it is related to its ability to store electrical energy. Based on Figure 3b, plotting the dielectric constant as a function of the temperature, BaTiO<sub>3</sub> exhibits phase transitions from an orthorhombic phase to a tetragonal phase at 22 °C and from a ferroelectric tetragonal phase to a paraelectric cubic phase at 132 °C, which suggests that

the BaTiO<sub>3</sub> is a typically ferroelectric material with remanent polarization along the [001] axis at room temperature [37,38].

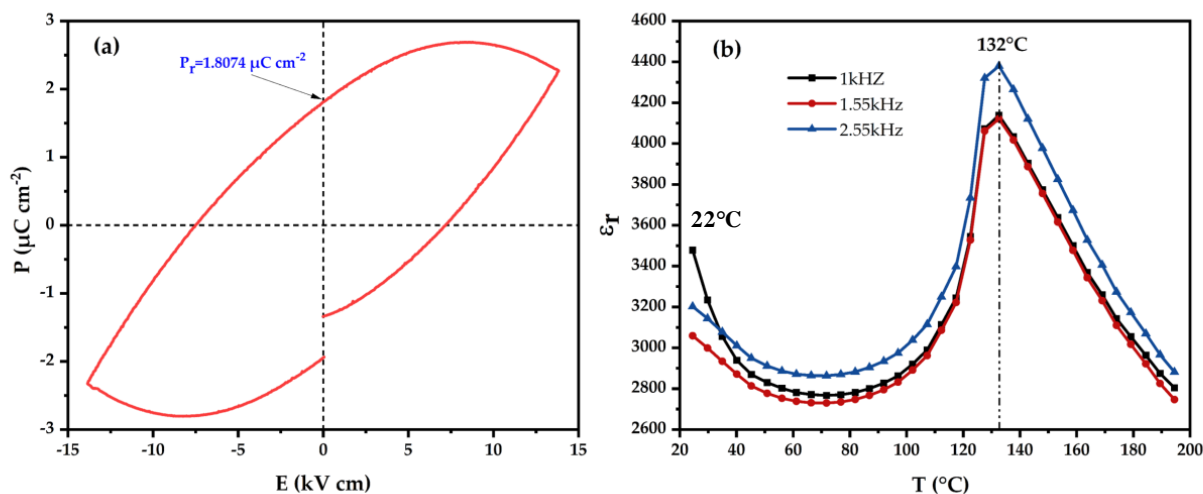


**Figure 3.** (a) P-E hysteresis loop of BaTiO<sub>3</sub>. (b) Temperature dependences of dielectric response of BaTiO<sub>3</sub> at 1 KHz, 1.55 KHz and 2.55 KHz.

## 2.2. Optical Properties

The absorption spectrum of the BaTiO<sub>3</sub> material was measured to provide information about its electronic structure. The absorption edge recorded at 285 nm is due to the electronic transitions between the valence and the conduction bands of the studied material. This transition is known as an interband transition and indicates the band gap of the BT. It should be noted that the band gap of the material is an essential property because it is related to the energy required for an electron to be excited from the valence band to the conduction band. A larger band gap indicates higher energy required for excitation, which can affect the photocatalytic activity of the material.

Tauc's plot, also shown in Figure 4, is a graphical representation of the absorption coefficient of the material as a function of the photon energy. Generally, the intersection with the x-axis of the linear part of this curve gives access to the band gap of the material. The Tauc's plot of the BaTiO<sub>3</sub> material confirms that the band gap is around 3.77 eV, which is consistent with the value obtained from the absorption spectrum and comparable to what was found in a previous work [39].

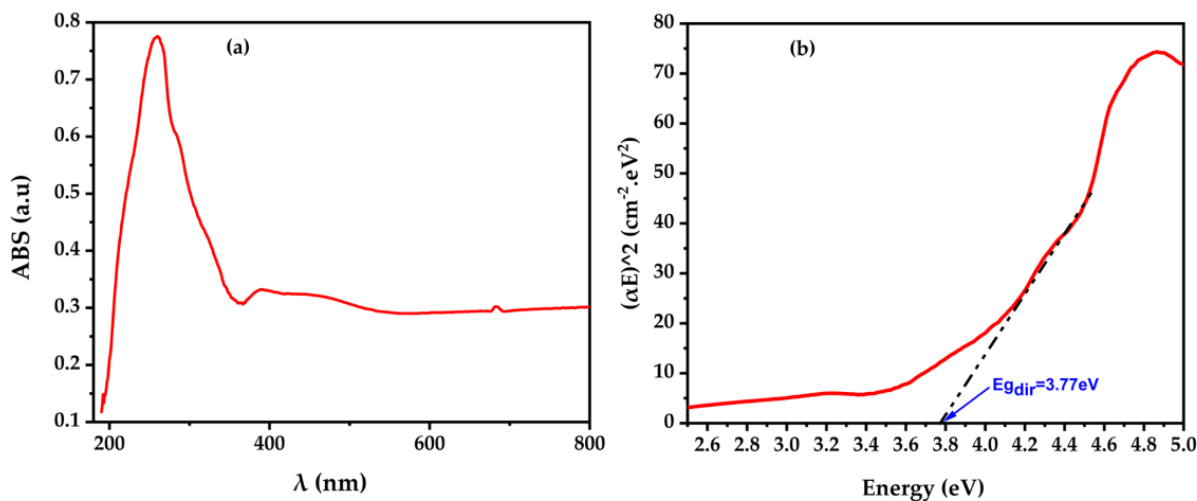


**Figure 4.** UV-visible absorbance of BaTiO<sub>3</sub> (a) and Tauc's plot (b).



Thus, the optical properties of the BT material indicate that it has a band gap of 3.77 eV, which suggests that the material would be active in the UV light region. This makes the material suitable for various applications such as photocatalysis, solar cells and optoelectronics. However, it should be noted that the material's optical properties alone are insufficient to fully assess its photocatalytic activity. Further studies, such as on photocatalytic activity, were performed in an air-cathode MFC to confirm this.

### 2.3. Electrochemical Characterization

Cyclic voltammetry (CV) was employed to investigate the nature of the processes occurring at the surface of the electrode and at the interface with the solution (denoised water or wastewater). The characteristics of the mixture of dairy industry and domestic wastewater used as a feedstock for the MFCs are listed in Materials and Methods, Section 3.

Figure 5a,b exhibit the voltammograms of the BT material with a scan rate variation from  $20 \text{ mV s}^{-1}$  to  $100 \text{ mV s}^{-1}$ . We observed an increase in the redox current intensity by increasing the scan rate, in accordance with the literature [40,41]. Furthermore, the BT-based electrode demonstrated a larger electroactive zone in wastewater than in the denoised medium, suggesting a potential application for wastewater treatment and power generation in MFC devices. The voltammogram size of BT is in agreement with other works when graphite electrodes were used in MFC systems for wastewater treatment [6,42].

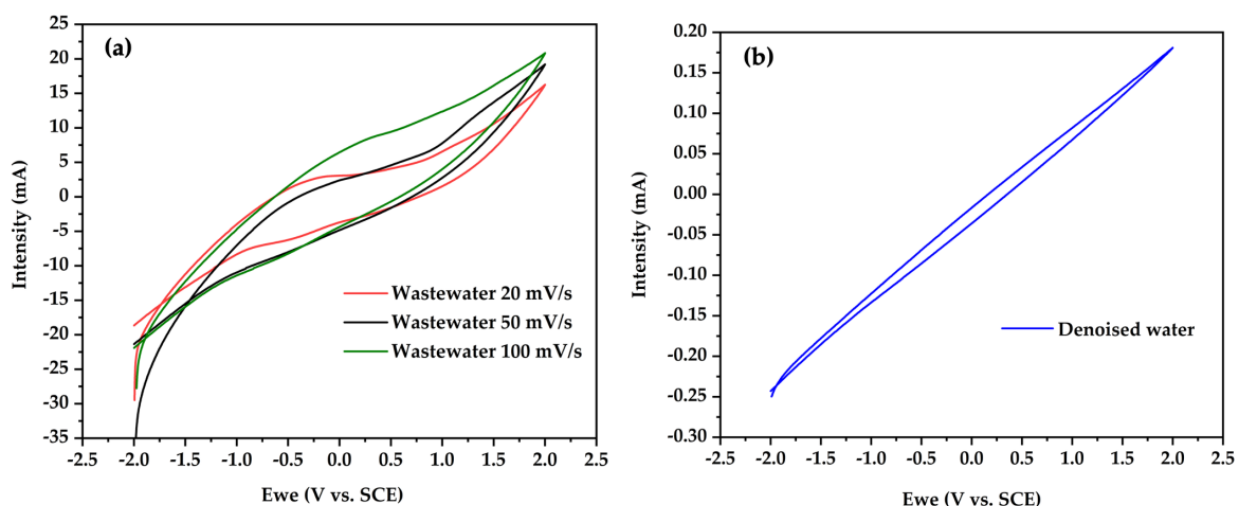


**Figure 5.** Cyclic voltammograms of  $\text{BaTiO}_3$  catalyst at different scan rates in (a) wastewater and (b) denoised water.

### 2.4. Performance in Single-Chamber MFC

Experiments were performed to analyze the photoelectrocatalytic activity of  $\text{BaTiO}_3$ , using it for the first time in an MFC as a photocathode. Figure 6a,b show the power and polarization curves of an MFC equipped with a cathode coated with BT, after 120 h in operation and in the presence and absence of light conditions. When the BT-based cathode was exposed to UV–visible light, the open circuit voltage (OCV) of the MFC system increased from 280 mV to 387 mV. The dependence of the polarization curve of the MFC is illustrated in Figure 6a. Both graph plots (BT with/without light source) show three potential loss zones, generally observed for MFCs, which are the activation loss, the ohmic loss and the concentration loss [43].

Power density data were a key parameter for evaluating MFC system behavior. The MFC with a BT-irradiated cathode presents the best MFC performance with a maximum power density of  $498 \text{ mW m}^{-2}$  associated with a current density of  $2408 \text{ mA m}^{-2}$ , which is 7.8 times higher than that of an MFC functioning with BT without irradiation ( $64.02 \text{ mW m}^{-2}$ ,  $1440 \text{ mA m}^{-2}$ ) (Figure 6b). This power performance is due to the photoelectrocatalytic activity of the  $\text{BaTiO}_3$  material. These results are very encouraging compared

to the various Pt-based cathodes recognized as potential catalysts used in microbial fuel cells [12,44,45].

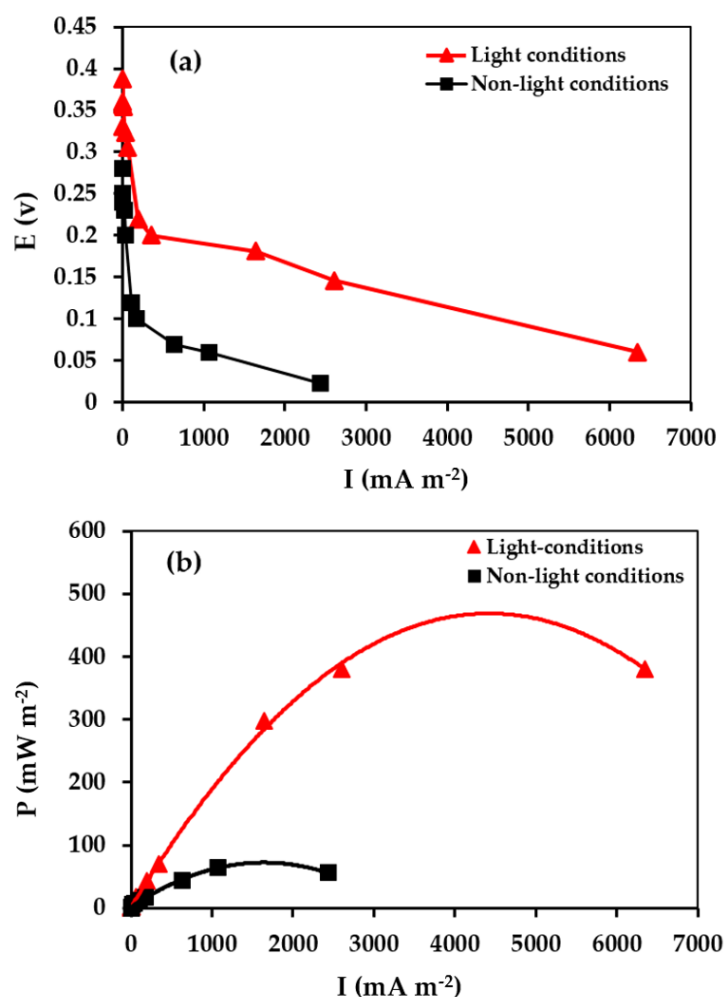


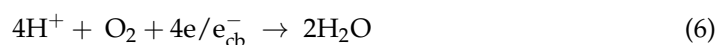
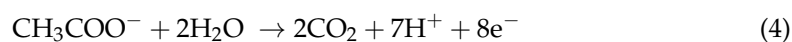
Figure 6. (a) Polarization curves (b) and power density for BaTiO<sub>3</sub>.

Recently, various ferroelectric photocatalytic materials have also been applied as cathodes in MFCs. BiFeO<sub>3</sub>-based cathodes, in the form of nanoparticles synthesized by the hydrothermal method, achieved a maximum power output of 332 mW m<sup>-2</sup> [46], that is lower than the value measured for BaTiO<sub>3</sub>-based cathodes studied in this work. On the other hand, cathodes based on non-stoichiometric ferroelectric materials such as iso-type LiMO<sub>3</sub> (M = Nb, Ta) modified by Cu<sup>2+</sup>, Mg<sup>2+</sup> were investigated [19–21]; their performance as photocatalysts in air-cathode MFCs was inferior to that of the present BaTiO<sub>3</sub> material. Moreover, it is worth mentioning that other types of TiO<sub>2</sub> cathode, the most well-known photocatalyst, led to a power output in this device in the (4.34–239) mW m<sup>-2</sup> range, which also remains significantly lower than that obtained with the BaTiO<sub>3</sub>-based configuration [47–51].

In the MFC, at the bioanode, the degradation of organic substrate can generate bioelectrons (e<sup>-</sup>) and inorganic matter through active microorganisms, taking as an example the oxidation of acetate (as shown in Equation (4)). These electrons accumulated in the bioanode are then transferred by an external charge driven by the potential difference in the MFC to reach the photocathode, and protons migrate to the photocathode surface via a proton exchange membrane (as shown in Equation (6)) where photoelectrocatalysis process occur.

In this study, the photocathode was coated with BaTiO<sub>3</sub> nanoparticles. When exposed to light, the electrons in the valence band of BaTiO<sub>3</sub> are excited to the conduction band, while the holes are retained in the valence band (as shown in Equation (5)). Additionally,

holes can combine with electrons from the anode to generate an electric current (as shown in Equation (7)) and decrease the rate of recombination of electron–hole pairs.



In addition, the spontaneous polarization in this material, along the *c*-axis, is due to a small ionic displacement mostly dominated by Ti ion displacement with respect to the oxygen [27,28]. This can improve the transport of photoinduced electron–hole charge carriers to the catalyst interfaces that were separated by the spontaneous polarization. Ferroelectric/electrode interfaces in any metal/semiconductor contact are known to generate defects which may change redox activity at the junction between deposited material and the support of the electrode [52]. A large number of charged defects are usually observed at the near surface of a ferroelectric-type material such as BaTiO<sub>3</sub> as, for many kinds of semiconductive metal, oxides may change the structure and polarization of ultrathin BaTiO<sub>3</sub>-coated cathodes. Therefore, the ORR can be promoted at the positively charged surface of the material.

COD removal efficiency is an important indicator of MFC performance in terms of treatment efficiency and energy production. Catalysts with better ORR performance require more electrons for oxygen reduction reactions. Accordingly, MFCs are expected to actively decompose organic substrates. The results of the present study indicated that all MFCs equipped with a BT-coated cathode had high COD removal efficiency in the presence and absence of light (Table 1). When the BT-based cathode was exposed to UV–visible light, a significant COD reduction was obtained, reaching 90%. However, the non-irradiation MFC system only achieved 74.5% COD removal. This COD removal value demonstrates a good correlation with the maximum power density results that increased from 64 mW m<sup>−2</sup> to 498 mW m<sup>−2</sup> in the absence and presence of UV–visible light, respectively.

**Table 1.** Performance of MFCs equipped with BaTiO<sub>3</sub> ceramic cathode in the presence and absence of light.

BaTiO <sub>3</sub> Sample	<sup>a</sup> Eg (eV)	P <sub>max</sub> (mW m <sup>−2</sup> )	I at P <sub>max</sub> (mA m <sup>−2</sup> )	OCV (mV)	<sup>b</sup> COD <sub>r</sub> after 120 h (%)
Absence of light	-	64.0	1440	280	74.5
Presence of light	3.77	498.0	2408.5	387	90

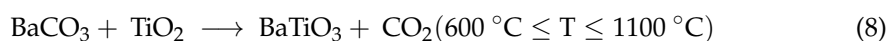
<sup>a</sup> Eg (eV): Energy gap. <sup>b</sup> COD<sub>r</sub>: Chemical oxygen demand removal.

Thus, we have demonstrated that the ferroelectric BaTiO<sub>3</sub> photocathode is a promising material for use in MFCs due to its ability to reduce COD and generate electricity.

### 3. Materials and Methods

#### 3.1. Catalyst Preparation and Characterization

BaTiO<sub>3</sub> (BT) powder was prepared following the solid-state synthesis by firing at high temperature a mixture of BaCO<sub>3</sub> (Merck, Darmstadt, Germany, 99%) and TiO<sub>2</sub> (Merck, Germany, 99%) (as shown in Equation (8)). The processing steps were: ball milling, calcining at 600 °C for 12 h to expel CO<sub>2</sub>, then increasing to 800, 1000 and 1100 °C for 12 h. The heat treatment was followed by slow cooling. The synthesized products were typically fine powders.





The crystalline structure of the BaTiO<sub>3</sub> was investigated by XRD analysis in the angular range 10–80° 2θ, by using a 0.02° step size and a scan speed of 0.05°/s. Diffraction patterns were registered with a Bruker D8 Advance diffractometer (Germany) equipped with monochromatic CuKα radiation (1.54 Å).

The morphology, composition and elemental mapping distribution of the BaTiO<sub>3</sub> compound were analyzed by scanning electron microscopy (SEM) and energy dispersive X-ray (EDX) analysis on QUATTRO S-FEG-Thermo Fisher equipment.

The powder of BaTiO<sub>3</sub> (BT) material was pressed (8 tons) into the form of discs, and then it was sintered at 1100 °C. The obtained pellet was metallized by silver lacquer and then the measurements of the dielectric characteristics were carried out using an impedance analyzer (Agilent 4294A) in the frequency range of 1Hz–35 KHz with an applied voltage of 500 mV in a temperature range of 20–200 °C.

The study of the optical properties was conducted through UV–visible–NIR diffuse reflectance spectroscopy at room temperature, covering the wavelength range of 190–1000 nm. A Varian Cary 5-E spectrometer (Australia) was used, equipped with an integrating sphere coated with polytetrafluoroethylene (PTFE) and a double monochromator.

The energy gap ( $E_g$ ) was estimated through performing the UV–Vis absorption analysis. The band gap of BaTiO<sub>3</sub> photocathode was calculated based on the Wood–Tauc method following Equation (9) [53–55]:

$$(\alpha h\nu)^2 = A(h\nu - E_g)^n \quad (9)$$

where  $\alpha$  represents the absorption coefficient,  $h$  and  $\nu$  are the Planck constant and the incident light frequency, respectively,  $A$  is a constant. The factor  $n$  in the equation is dependent on the type of electron transition and is either equal to 1/2 or 2 for direct and indirect band gap transitions, respectively.

The electrochemical measurements were performed using a potentiostat (SP-150-BioLogic science instruments, French, Grenoble) equipped with EC-Lab software. The system contained three electrodes, specifically a working electrode, a reference electrode based on saturated calomel and a counter-electrode in the form of a platinum wire. The influence of scan rate variation was examined using cyclic voltammetry in denoised water and wastewater.

### 3.2. MFC Operation

The synthesized BaTiO<sub>3</sub> ceramic were evaluated in air-cathode MFCs constituted by single reactors of 250 mL anode capacity and equipped with an external jacket, to control the operating temperature at 27 °C. The cathode was composed of a mixture of the synthesized BaTiO<sub>3</sub> phases as catalysts and a solution of polytetrafluoroethylene (PTFE) (solid, Sigma-Aldrich, Burlington, MA, USA) as binder. The mixture was mechanically pressed onto a piece of carbon cloth with a surface area of 1 cm<sup>2</sup>. The total mass was 60 mg/cm<sup>2</sup> in a 1:9 mass ratio of PTFE:catalyst. The anode consisted of 100 g of graphite granules (Graphite Store, IL, USA) with a diameter of 2–6 mm and a graphite rod (Graphite Store, USA) with a diameter of 3.18 mm, which was connected to the cathode with an external resistance of 1 kΩ. The anode chamber was filled with a mixture of dairy industry and domestic wastewater (125 mL) whose characteristics are listed in Table 2. The reactors were installed with a Nafion-type proton exchange membrane with a diameter of 3.8 cm located between the air-cathode and the anode chamber [56]. The experiment was performed for 120 h, under UV–visible light irradiation using a 500W power lamp.

The polarization and power measurements were obtained from the variation of different external resistors (11 MΩ–1 Ω). The open circuit voltages (OCVs) of the MFCs were measured with a voltmeter. The current ( $I$ ) and power ( $P$ ) densities were obtained by the equations:  $I = V/R$  and  $P = V^2/R$ , where  $V$  is the cell voltage and  $R$  is an external resistance, normalized to the surface of the cathode.

**Table 2.** The physico-chemical parameters of wastewater before testing in single-chamber MFC.

	COD (mg L <sup>-1</sup> )	<sup>a</sup> BOD (mg L <sup>-1</sup> )	Dissolved Oxygen (mg L <sup>-1</sup> )	<sup>b</sup> EC (μS cm <sup>-1</sup> )	pH	Temperature (°C)
Wastewater tested	2500	440	0.8	4330	7.8	27

<sup>a</sup> BOD: Biochemical oxygen demand. <sup>b</sup> EC: Electrical conductivity.

### 3.3. COD Removal Efficiency

The chemical oxygen demand (COD) was determined using the APHA standard method [57] on a photoLab 7600 UV–visible spectrophotometer (WTW, Germany) and determined with Equation (9):

$$\% \text{ COD}_r = \frac{[\text{COD}]_i - [\text{COD}]_f}{[\text{COD}]_i} \times 100 \quad (10)$$

where  $[\text{COD}]_i$  (mg/L) = initial COD charge in the wastewater inlet to the anode chamber and  $[\text{COD}]_f$  (mg/L) = COD of the effluent in the anode chamber at the end of the experiment.

## 4. Conclusions

This work investigated for the first time the possible application of BaTiO<sub>3</sub> (BT) as a cathode material for microbial fuel cells (MFCs), in the presence and absence of a UV–Vis light source, using a mixture of dairy industry and domestic wastewater as feedstock.

The energy performance of BT was significantly improved when the MFC was working under light conditions. The maximum power densities generated by the MFC using BT-based cathodes increased from 64 mW m<sup>-2</sup> to 698 mW m<sup>-2</sup> in the absence and presence of UV–visible light, respectively. The BT-based MFC also exhibited a remarkable COD removal performance, with a maximum of 90% obtained in the presence of a light source.

The BT compares well with other alternative ferroelectric cathode materials reported in the literature for MFC devices.

In conclusion, this work demonstrated the feasibility of a sustainable process for energy production, by using as cathodic material, in MFCs, BaTiO<sub>3</sub> that is a functional and cost-effective ferroelectric perovskite, able to convert organic matter into electrical energy while simultaneously purifying water.

**Author Contributions:** All the authors have contributed to the achievement of this work. N.T. and A.B. provided preparation and characterization of the catalyst, performed experiments and wrote parts of the paper; N.L. and Y.E.H. helped with characterization techniques; M.E.M. is the Head of the ENSAM Research Team and oversaw investigation and validation; E.M.L. helped to find resources; M.K. designed the catalyst; J.T. finalized the writing of the manuscript; L.F.L. contributed to funding the research and completed the writing of the manuscript in its final form. All authors have read and agreed to the published version of the manuscript.

**Funding:** This work was financially supported by the Moroccan Ministry of Higher Education, Scientific Research and Innovation, and the OCP Foundation through the APRD research program.

**Institutional Review Board Statement:** Not applicable.

**Informed Consent Statement:** Not applicable.

**Data Availability Statement:** All the data are included in the article.

**Acknowledgments:** We would like to thank the Moroccan Ministry of Higher Education, Scientific Research and Innovation, and the OCP Foundation who funded this work through the APRD research program. Part of this research was carried out by L.F.L. in COST ACTION CA 18224 GREENERING “Green Chemical Engineering Network towards upscaling Sustainable Processes”, and COST Action

CA20127 “Waste biorefinery technologies for accelerating sustainable energy processes”, supported by European Cooperation in Science and Technology (COST).

**Conflicts of Interest:** The authors declare no conflict of interest.

## References

1. Logan, B.E.; Hamelers, B.; Rozendal, R.; Schröder, U.; Keller, J.; Freguia, S.; Aelterman, P.; Verstraete, W.; Rabaey, K. Microbial Fuel Cells: Methodology and Technology. *Environ. Sci. Technol.* **2006**, *40*, 5181–5192. [[CrossRef](#)] [[PubMed](#)]
2. Srivastava, R.K.; Boddula, R.; Pothu, R. Microbial fuel cells: Technologically advanced devices and approach for sustainable/renewable energy development. *Energy Convers. Manag. X* **2022**, *13*, 100160. [[CrossRef](#)]
3. Tang, J.; Xu, X.; Tang, T.; Zhong, Y.; Shao, Z. Perovskite-Based Electrocatalysts for Cost-Effective Ultrahigh-Current-Density Water Splitting in Anion Exchange Membrane Electrolyzer Cell. *Small Methods* **2022**, *6*, 2201099. [[CrossRef](#)] [[PubMed](#)]
4. Li, M.; Zhou, M.; Tian, X.; Tan, C.; McDaniel, C.T.; Hassett, D.J.; Gu, T. Microbial fuel cell (MFC) power performance improvement through enhanced microbial electrogenicity. *Biotechnol. Adv.* **2018**, *36*, 1316–1327. [[CrossRef](#)]
5. Kouam Ida, T.; Mandal, B. Microbial fuel cell design, application and performance: A review. *Mater. Today Proc.* **2022**, *in press*. [[CrossRef](#)]
6. Benzaouak, A.; Touach, N.; Mahir, H.; Elhamdouni, Y.; Labjar, N.; El Hamidi, A.; El Mahi, M.; Lotfi, E.M.; Kacimi, M.; Liotta, L.F. ZrP2O7 as a Cathodic Material in Single-Chamber MFC for Bioenergy Production. *Nanomaterials* **2022**, *12*, 3330. [[CrossRef](#)]
7. Touach, N.; Ortiz-Martínez, V.M.; Salar-García, M.J.; Benzaouak, A.; Hernández-Fernández, F.; de los Ríos, A.P.; Labjar, N.; Louki, S.; El Mahi, M.; Lotfi, E.M. Influence of the preparation method of MnO<sub>2</sub>-based cathodes on the performance of single-chamber MFCs using wastewater. *Sep. Purif. Technol.* **2016**, *171*, 174–181. [[CrossRef](#)]
8. Fan, M.; Li, H.; Mo, J.; Chen, Y.; Liu, J.; Zhu, J.; Shen, S. Performance comparison of activated carbon and Pt/C cathode microbial fuel cells on sulfamethoxazole degradation: Effect of salinity and mechanism study. *J. Clean. Prod.* **2022**, *375*, 134018. [[CrossRef](#)]
9. Touach, N.; Ortiz-Martínez, V.M.; Salar-García, M.J.; Benzaouak, A.; Hernández-Fernández, F.; de Ríos, A.P.; El Mahi, M.; Lotfi, E.M. On the use of ferroelectric material LiNbO<sub>3</sub> as novel photocatalyst in wastewater-fed microbial fuel cells. *Particuology* **2017**, *34*, 147–155. [[CrossRef](#)]
10. Zhao, K.; Shu, Y.; Li, F.; Peng, G. Bimetallic catalysts as electrocatalytic cathode materials for the oxygen reduction reaction in microbial fuel cell: A review. *Green Energy Environ.* **2022**, *in press*. [[CrossRef](#)]
11. Zeng, L.Z.; Zhao, S.F.; Wang, Y.Q.; Li, H.; Li, W.S. Ni/β-Mo<sub>2</sub>C as noble-metal-free anodic electrocatalyst of microbial fuel cell based on *Klebsiella pneumoniae*. *Int. J. Hydrog. Energy* **2012**, *37*, 4590–4596. [[CrossRef](#)]
12. Peera, S.G.; Maiyalagan, T.; Liu, C.; Ashmath, S.; Lee, T.G.; Jiang, Z.; Mao, S. A review on carbon and non-precious metal based cathode catalysts in microbial fuel cells. *Int. J. Hydrog. Energy* **2021**, *46*, 3056–3089. [[CrossRef](#)]
13. Chen, C.-F.; King, G.; Dickerson, R.M.; Papin, P.A.; Gupta, S.; Kellogg, W.R.; Wu, G. Oxygen-deficient BaTiO<sub>3-x</sub> perovskite as an efficient bifunctional oxygen electrocatalyst. *Nano Energy* **2015**, *13*, 423–432. [[CrossRef](#)]
14. Yang, L.; Jiao, Y.; Xu, X.; Pan, Y.; Su, C.; Duan, X.; Sun, H.; Liu, S.; Wang, S.; Shao, Z. Superstructures with Atomic-Level Arranged Perovskite and Oxide Layers for Advanced Oxidation with an Enhanced Non-Free Radical Pathway. *ACS Sustain. Chem. Eng.* **2022**, *10*, 1899–1909. [[CrossRef](#)]
15. Jin, C.; Cao, X.; Lu, F.; Yang, Z.; Yang, R. Electrochemical study of Ba<sub>0.5</sub>Sr<sub>0.5</sub>Co<sub>0.8</sub>Fe<sub>0.2</sub>O<sub>3</sub> perovskite as bifunctional catalyst in alkaline media. *Int. J. Hydrog. Energy* **2013**, *38*, 10389–10393. [[CrossRef](#)]
16. Xu, X.; Wang, W.; Zhou, W.; Shao, Z. Recent Advances in Novel Nanostructuring Methods of Perovskite Electrocatalysts for Energy-Related Applications. *Small Methods* **2018**, *2*, 1800071. [[CrossRef](#)]
17. Ali, S.M.; Abd Al-Rahman, Y.M.; Galal, A. Catalytic Activity toward Oxygen Evolution of LaFeO<sub>3</sub> Prepared by the Microwave Assisted Citrate Method. *J. Electrochem. Soc.* **2012**, *159*, F600. [[CrossRef](#)]
18. Benzaouak, A.; Touach, N.e.; Ortiz-Martínez, V.M.; Salar-García, M.J.; Hernández-Fernández, F.J.; Perez de los Rios, A.; Mahi, M.E.; Lotfi, E.M. Ferroelectric LiTaO<sub>3</sub> as novel photo-electrocatalyst in microbial fuel cells. *Environ. Prog. Sustain. Energy* **2017**, *36*, 1568–1574. [[CrossRef](#)]
19. Louki, S.; Touach, N.; Benzaouak, A.; Ortiz-Martínez, V.; Salar-García, M.; Hernández-Fernández, F.; de los Ríos, A.; El Mahi, M.; Lotfi, E. Characterization of New Nonstoichiometric Ferroelectric (Li<sub>0.95</sub>Cu<sub>0.15</sub>)Ta<sub>0.76</sub>Nb<sub>0.19</sub>O<sub>3</sub> and Comparative Study With (Li<sub>0.95</sub>Cu<sub>0.15</sub>)Ta<sub>0.57</sub>Nb<sub>0.38</sub>O<sub>3</sub> as Photocatalysts in Microbial Fuel Cells. *J. Electrochem. Energy Convers. Storage* **2019**, *16*, 021009. [[CrossRef](#)]
20. Louki, S.; Touach, N.e.; Benzaouak, A.; Salar-García, M.J.; Ortiz-Martínez, V.M.; Hernández-Fernández, F.J.; de los Ríos, A.P.; El Mahi, M.; Lotfi, E.M. Preparation of new ferroelectric Li<sub>0.95</sub>Ta<sub>0.57</sub>Nb<sub>0.38</sub>Cu<sub>0.15</sub>O<sub>3</sub> materials as photocatalysts in microbial fuel cells. *Can. J. Chem. Eng.* **2018**, *96*, 1656–1662. [[CrossRef](#)]
21. Touach, N.; Benzaouak, A.; Toyir, J.; El Hamidi, A.; El Mahi, M.; Lotfi, E.M.; Kacimi, M.; Liotta, L.F. Bioenergy Generation and Wastewater Purification with Li<sub>0.95</sub>Ta<sub>0.76</sub>Nb<sub>0.19</sub>Mg<sub>0.15</sub>O<sub>3</sub> as New Air-Photocathode for MFCs. *Catalysts* **2022**, *12*, 1424. [[CrossRef](#)]
22. Briscoe, J.; Dunn, S. Piezoelectricity and ferroelectricity. In *Nanostructured Piezoelectric Energy Harvesters*; Springer: Berlin/Heidelberg, Germany, 2014; pp. 3–17.

23. Dasireddy, V.D.B.C.; Likoza, B. Photocatalytic CO<sub>2</sub> reduction to methanol over bismuth promoted BaTiO<sub>3</sub> perovskite nanoparticle catalysts. *Renew. Energy* **2022**, *195*, 885–895. [[CrossRef](#)]
24. Shiozaki, R.; Andersen, A.G.; Hayakawa, T.; Hamakawa, S.; Suzuki, K.; Shimizu, M.; Takehira, K. Partial oxidation of methane over a Ni/BaTiO<sub>3</sub> catalyst prepared by solid phase crystallization. *J. Chem. Soc. Faraday Trans.* **1997**, *93*, 3235–3242. [[CrossRef](#)]
25. Wang, Z.; Lin, J.; Wang, R.; Wei, K. Ammonia synthesis over ruthenium catalyst supported on perovskite type BaTiO<sub>3</sub>. *Catal. Commun.* **2013**, *32*, 11–14. [[CrossRef](#)]
26. Wang, B.; Yao, S.; Peng, Y.; Xu, Y. Toluene removal over TiO<sub>2</sub>-BaTiO<sub>3</sub> catalysts in an atmospheric dielectric barrier discharge. *J. Environ. Chem. Eng.* **2018**, *6*, 3819–3826. [[CrossRef](#)]
27. Li, L.; Salvador, P.A.; Rohrer, G.S. Photocatalysts with internal electric fields. *Nanoscale* **2014**, *6*, 24–42. [[CrossRef](#)]
28. Khan, M.A.; Nadeem, M.A.; Idriss, H. Ferroelectric polarization effect on surface chemistry and photo-catalytic activity: A review. *Surf. Sci. Rep.* **2016**, *71*, 1–31. [[CrossRef](#)]
29. Giocondi, J.L.; Rohrer, G.S. Spatial separation of photochemical oxidation and reduction reactions on the surface of ferroelectric BaTiO<sub>3</sub>. *J. Phys. Chem. B* **2001**, *105*, 8275–8277. [[CrossRef](#)]
30. Chen, L.; Li, H.; Wu, Z.; Feng, L.; Yu, S.; Zhang, H.; Gao, J.; Mai, Y.-W.; Jia, Y. Enhancement of pyroelectric catalysis of ferroelectric BaTiO<sub>3</sub> crystal: The action mechanism of electric poling. *Ceram. Int.* **2020**, *46*, 16763–16769. [[CrossRef](#)]
31. Kappadan, S.; Gebreab, T.W.; Thomas, S.; Kalarikkal, N. Tetragonal BaTiO<sub>3</sub> nanoparticles: An efficient photocatalyst for the degradation of organic pollutants. *Mater. Sci. Semicond. Process.* **2016**, *51*, 42–47. [[CrossRef](#)]
32. Devi, L.G.; Nithya, P.M. Preparation, characterization and photocatalytic activity of BaTiF<sub>6</sub> and BaTiO<sub>3</sub>: A comparative study. *J. Environ. Chem. Eng.* **2018**, *6*, 3565–3573. [[CrossRef](#)]
33. Devi, L.G.; Nithya, P. Photocatalytic activity of Hemin (Fe (III) porphyrin) anchored BaTiO<sub>3</sub> under the illumination of visible light: Synergetic effects of photosensitization, photo-Fenton & photocatalysis processes. *Inorg. Chem. Front.* **2018**, *5*, 127–138.
34. Xia, Y.; Jia, Y.; Qian, W.; Xu, X.; Wu, Z.; Han, Z.; Hong, Y.; You, H.; Ismail, M.; Bai, G.; et al. Pyroelectrically Induced Pyro-Electro-Chemical Catalytic Activity of BaTiO<sub>3</sub> Nanofibers under Room-Temperature Cold–Hot Cycle Excitations. *Metals* **2017**, *7*, 122. [[CrossRef](#)]
35. Liu, X.; Xiao, L.; Zhang, Y.; Sun, H. Significantly enhanced piezo-photocatalytic capability in BaTiO<sub>3</sub> nanowires for degrading organic dye. *J. Mater.* **2020**, *6*, 256–262. [[CrossRef](#)]
36. Xu, X.; Wu, Z.; Jia, Y.; Li, W.; Liu, Y.; Zhang, Y.; Xue, A.X. Multiferroic properties of nanopowder-synthesized ferroelectric-ferromagnetic 0.6 BaTiO<sub>3</sub>-0.4 NiFe<sub>2</sub>O<sub>4</sub> ceramic. *J. Nanomater.* **2015**, *16*, 231.
37. Masekela, D.; Hintsho-Mbita, N.C.; Sam, S.; Yusuf, T.L.; Mabuba, N. Application of BaTiO<sub>3</sub>-based catalysts for piezocatalytic, photocatalytic and piezo-photocatalytic degradation of organic pollutants and bacterial disinfection in wastewater: A comprehensive review. *Arab. J. Chem.* **2023**, *16*, 104473. [[CrossRef](#)]
38. Oliveira, M.C.; Ribeiro, R.A.P.; Longo, E.; Bomio, M.R.D.; Motta, F.V.; de Lazaro, S.R. Temperature dependence on phase evolution in the BaTiO<sub>3</sub> polytypes studied using ab initio calculations. *Int. J. Quantum Chem.* **2020**, *120*, e26054. [[CrossRef](#)]
39. Li, G.; Xie, J.; Wang, J.; Xia, L.; Li, Y.; Hu, W. Nanoscale Surface Disorder for Enhanced Solar Absorption and Superior Visible-Light Photocatalytic Property in Ti-Rich BaTiO<sub>3</sub> Nanocrystals. *ACS Omega* **2019**, *4*, 9673–9679. [[CrossRef](#)]
40. Charoen-amornkitt, P.; Suzuki, T.; Tsushima, S. Ohmic resistance and constant phase element effects on cyclic voltammograms using a combined model of mass transport and equivalent circuits. *Electrochim. Acta* **2017**, *258*, 433–441. [[CrossRef](#)]
41. Hermouche, L.; Aqil, Y.; Abbi, K.; El Hamdouni, Y.; Ouanji, F.; El Hajjaji, S.; El Mahi, M.; Lotfi, E.m.; Labjar, N. Eco-friendly modified carbon paste electrode by Bigarreau Burlat kernel shells for simultaneous trace detection of cadmium, lead, and copper. *Chem. Data Collect.* **2021**, *32*, 100642. [[CrossRef](#)]
42. Veer Raghavulu, S.; Venkata Mohan, S.; Venkateswar Reddy, M.; Mohanakrishna, G.; Sarma, P.N. Behavior of single chambered mediatorless microbial fuel cell (MFC) at acidophilic, neutral and alkaline microenvironments during chemical wastewater treatment. *Int. J. Hydrogen Energy* **2009**, *34*, 7547–7554. [[CrossRef](#)]
43. Choudhury, P.; Bhunia, B.; Mahata, N.; Bandyopadhyay, T.K. Optimization for the improvement of power in equal volume of single chamber microbial fuel cell using dairy wastewater. *J. Indian Chem. Soc.* **2022**, *99*, 100489. [[CrossRef](#)]
44. Ghasemi, M.; Sedighi, M.; Tan, Y.H. Carbon nanotube/Pt cathode nanocomposite electrode in microbial fuel cells for wastewater treatment and bioenergy production. *Sustainability* **2021**, *13*, 8057. [[CrossRef](#)]
45. Chaturvedi, A.; Kundu, P.P. Recent advances and perspectives in platinum-free cathode catalysts in microbial fuel cells. *J. Environ. Chem. Eng.* **2021**, *9*, 105662. [[CrossRef](#)]
46. Lam, S.-M.; Sin, J.-C.; Zeng, H.; Lin, H.; Li, H.; Mohamed, A.R.; Lim, J.W. Ameliorating Cu<sup>2+</sup> reduction in microbial fuel cell with Z-scheme BiFeO<sub>3</sub> decorated on flower-like ZnO composite photocathode. *Chemosphere* **2022**, *287*, 132384. [[CrossRef](#)] [[PubMed](#)]
47. Ali Ansari, S.; Mansoob Khan, M.; Omaish Ansari, M.; Hwan Cho, M. Improved electrode performance in microbial fuel cells and the enhanced visible light-induced photoelectrochemical behaviour of PtOx@M-TiO<sub>2</sub> nanocomposites. *Ceram. Int.* **2015**, *41*, 9131–9139. [[CrossRef](#)]
48. Ma, J.; Chen, D.; Zhang, W.; An, Z.; Zeng, K.; Yuan, M.; Shen, J. Enhanced performance and degradation of wastewater in microbial fuel cells using titanium dioxide nanowire photocathodes. *RSC Adv.* **2021**, *11*, 2242–2252. [[CrossRef](#)]
49. Bhowmick, G.D.; Noori, M.T.; Das, I.; Neethu, B.; Ghangrekar, M.M.; Mitra, A. Bismuth doped TiO<sub>2</sub> as an excellent photocathode catalyst to enhance the performance of microbial fuel cell. *Int. J. Hydrogen Energy* **2018**, *43*, 7501–7510. [[CrossRef](#)]

50. Bhowmick, G.D.; Chakraborty, I.; Ghangrekar, M.M.; Mitra, A. TiO<sub>2</sub>/Activated carbon photo cathode catalyst exposed to ultraviolet radiation to enhance the efficacy of integrated microbial fuel cell-membrane bioreactor. *Bioresour. Technol. Rep.* **2019**, *7*, 100303. [[CrossRef](#)]
51. He, Y.; Chen, K.; Leung, M.K.H.; Zhang, Y.; Li, L.; Li, G.; Xuan, J.; Li, J. Photocatalytic fuel cell—A review. *Chem. Eng. J.* **2022**, *428*, 131074. [[CrossRef](#)]
52. Chang, L.; McMillen, M.; Gregg, J. The influence of point defects and inhomogeneous strain on the functional behavior of thin film ferroelectrics. *Appl. Phys. Lett.* **2009**, *94*, 212905. [[CrossRef](#)]
53. Wood, D.; Tauc, J. Weak absorption tails in amorphous semiconductors. *Phys. Rev. B* **1972**, *5*, 3144. [[CrossRef](#)]
54. Tauc, J.; Grigorovici, R.; Vancu, A. Optical properties and electronic structure of amorphous germanium. *Phys. Status Solidi* **1966**, *15*, 627–637. [[CrossRef](#)]
55. Viezbicke, B.D.; Patel, S.; Davis, B.E.; Birnie III, D.P. Evaluation of the Tauc method for optical absorption edge determination: ZnO thin films as a model system. *Phys. Status Solidi* **2015**, *252*, 1700–1710. [[CrossRef](#)]
56. Hernández-Fernández, F.J.; Pérez de los Ríos, A.; Mateo-Ramírez, F.; Godínez, C.; Lozano-Blanco, L.J.; Moreno, J.I.; Tomás-Alonso, F. New application of supported ionic liquids membranes as proton exchange membranes in microbial fuel cell for waste water treatment. *Chem. Eng. J.* **2015**, *279*, 115–119. [[CrossRef](#)]
57. Larrosa-Guerrero, A.; Scott, K.; Head, I.M.; Mateo, F.; Ginesta, A.; Godínez, C. Effect of temperature on the performance of microbial fuel cells. *Fuel* **2010**, *89*, 3985–3994. [[CrossRef](#)]

**Disclaimer/Publisher’s Note:** The statements, opinions and data contained in all publications are solely those of the individual author(s) and contributor(s) and not of MDPI and/or the editor(s). MDPI and/or the editor(s) disclaim responsibility for any injury to people or property resulting from any ideas, methods, instructions or products referred to in the content.